

# Supporting Information

## **A Green Route to Fabricate MoS<sub>2</sub> Nanosheets in Water/ethanol/CO<sub>2</sub>**

**Yuhang Qi,<sup>a</sup> Nan Wang,<sup>a</sup> Qun Xu,<sup>\*a</sup> Hongxiang Li,<sup>a</sup> Pengshang Zhou,<sup>a</sup> Xin Lu<sup>b</sup> and Guoqiang Zhao<sup>b</sup>**

### Table of Contents

1. Experimental Section
2. Concentration of the samples with different volume fractions of ethanol
3. The schematic process
4. Phase behavior of emulsions the CO<sub>2</sub>/ethanol/water system
5. Optical characterization of MoS<sub>2</sub> dispersions
6. SEM images of MoS<sub>2</sub> nanosheets
7. Absorption spectra of MoS<sub>2</sub> supernatants with and without SC CO<sub>2</sub> assisted by exfoliation
8. XRD patterns and Raman spectra of bulk MoS<sub>2</sub> and few layers MoS<sub>2</sub>
9. The fluorescent images of lung cancer and human embryonic kidney cells stained with MoS<sub>2</sub> nanosheets

## Experimental Section

Materials: MoS<sub>2</sub> Powder was purchased from Sigma Aldrich (Fluka, Product Number: 69860). Ethanol used in all experiments was purchased from Sinopharm Chemical Reagent Co., Ltd. (China) and used without further purification. Aqueous solution was prepared with double-distilled water.

Exfoliation Process: MoS<sub>2</sub> powder (50 mg, 6-40mm, Sigma-Aldrich Reagent Inc.) was added to 50 mL flask. 10 mL of ethanol/water mixtures with ethanol volume fractions of 10 to 90 % were added as dispersion solvents. The dispersion in the sealed flask was sonicated in the bath for 2 h, and then the dispersion was then quickly transferred into the supercritical CO<sub>2</sub> apparatus composed mainly of a stainless steel autoclave (60 mL) with a heating jacket and a temperature controller. The autoclave was heated to 313.2 K, and CO<sub>2</sub> was then charged into the autoclave to the desired pressure under stirring. After a reaction time of 3 h, the gas was slowly released. Finally the dispersion was sonicated for 3 h, and then the dispersion was centrifuged at 3000 rpm for 15 mins to remove aggregates. The supernatant (top three quarters of the centrifuged dispersion) was collected by pipette.

Characterization: The morphologies of MoS<sub>2</sub> powder and sediment were characterized by field-emission SEM (JEOR JSM-6700F). Tapping-mode AFM (Nanoscope IIIA), HRTEM (JEOL JEM-2100F), and TEM (JEOL JEM-2100) were used to study the morphology of the nanomaterials. UV/Vis spectra (Shimadzu UV-240/PC) were measured to evaluate MoS<sub>2</sub> dispersions concentration. Raman spectra of MoS<sub>2</sub> samples were obtained with a 365 nm laser. The PL properties of MoS<sub>2</sub> nanosheets were investigated by PL spectra (Horiba Fluorolog-3).

**Table S1.** Concentration of the samples with different volume fractions of ethanol.

Volume fractions of Ethanol	Absorbance ( $A_{672\text{nm}}$ ) / $\text{cm}^{-1}$	Concentration / $\text{mg/mL}^{-1}$
10%	0.126	0.004
20%	0.241	0.008
30%	0.313	0.011
40%	0.459	0.015
50%	0.526	0.018
60%	0.493	0.017
70%	0.689	0.023
80%	0.911	0.030
90%	0.028	0.001

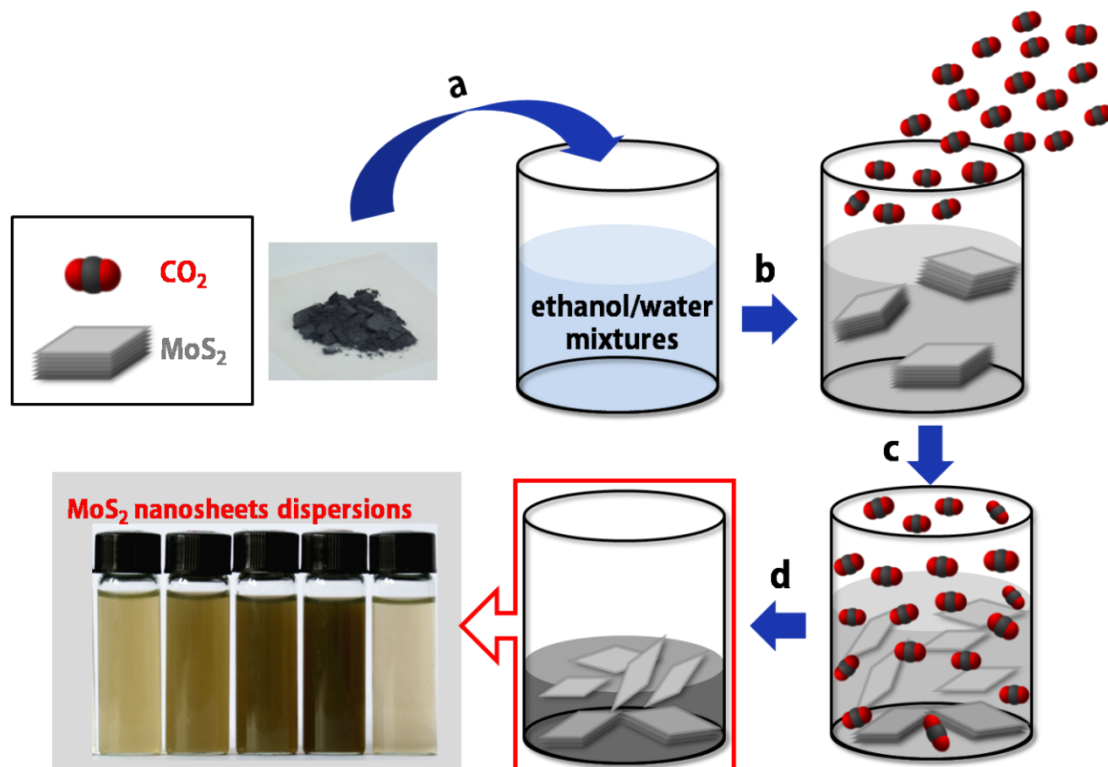


**Figure S1.** The schematic process to produce MoS<sub>2</sub> nanosheets from layered bulk materials in the CO<sub>2</sub>/ethanol/water system environment.

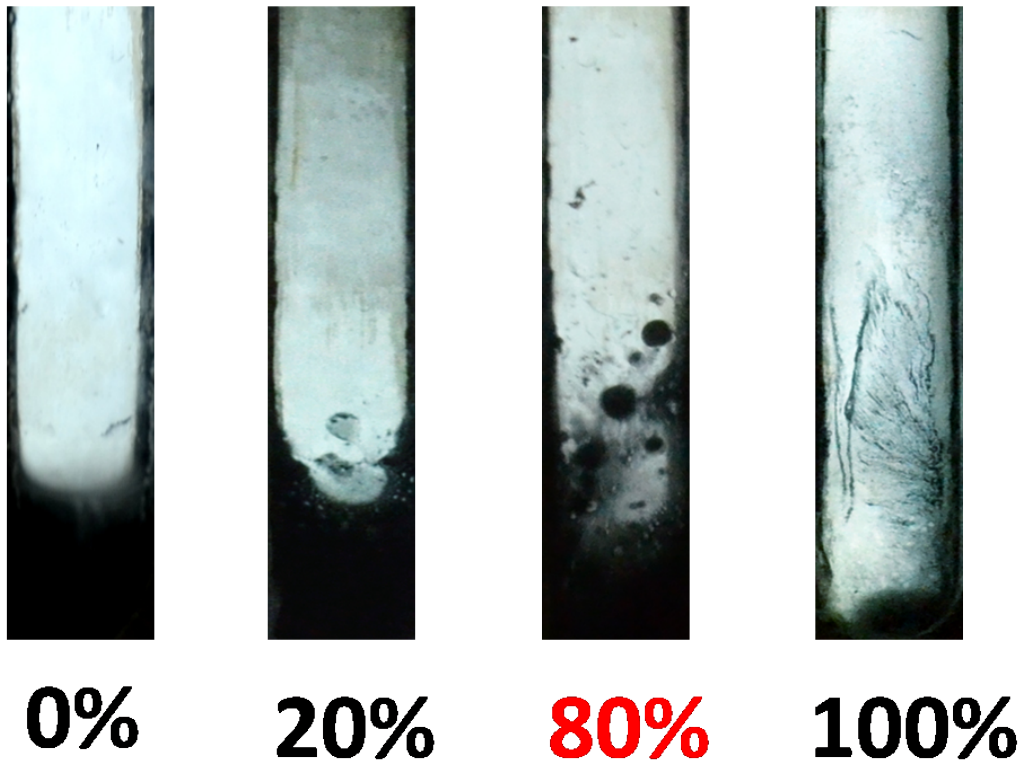


**Figure S2.** Phase behavior of emulsions the CO<sub>2</sub>/ethanol/water system. Photographs of the CO<sub>2</sub>/ethanol/water system with CO<sub>2</sub> pressures of 16 MPa at 313.2 K, ethanol volume fractions of (a) 0%, (b) 20%, (c) 80%, (d) 100%

In order to investigate the effects of the different volume fractions of ethanol on the exfoliation of MoS<sub>2</sub> in the SC CO<sub>2</sub>/ethanol/water system, the phase behavior of the system under the condition of CO<sub>2</sub> pressure at 16 MPa and temperature of 313.2 K, with different volume fraction of ethanol are studied. The experimental results are shown in Figure 2Sa-d. Figure S2a shows that bulk MoS<sub>2</sub> dispersed in pure water solution, and there were no splashing droplets with the high speed stir. With the increasing volume fraction of ethanol, a growing number of bubbles appeared in the upper part of water solution (Figure S2b). We found that only a few black droplets floating in the continuous CO<sub>2</sub> phase, which was similar to the formation of CO<sub>2</sub>-in-water pickering emulsion. The formation of the droplet is due to the dispersed MoS<sub>2</sub> existing at the interface of two phase system, which is driven by minimization of interfacial free energy of the system. It is known that the bulk MoS<sub>2</sub> have surface energies of ~40 mJ/m<sup>2</sup>, which lies between the surface tension of water ( $\gamma_w = 69.7$  mN/m at 313.2K) and the surface tension of supercritical CO<sub>2</sub> ( $\gamma_s \sim 0$  mN/m). Subsequently, with continuously increasing the volume fraction of ethanol, a growing number of black droplets existed in the continuous CO<sub>2</sub> phase (Figure S2c). However, when ethanol volume fraction reached 100%, there is no possibility to build the pickering emulsion, nor it is possible to perform the exfoliation of MoS<sub>2</sub>.

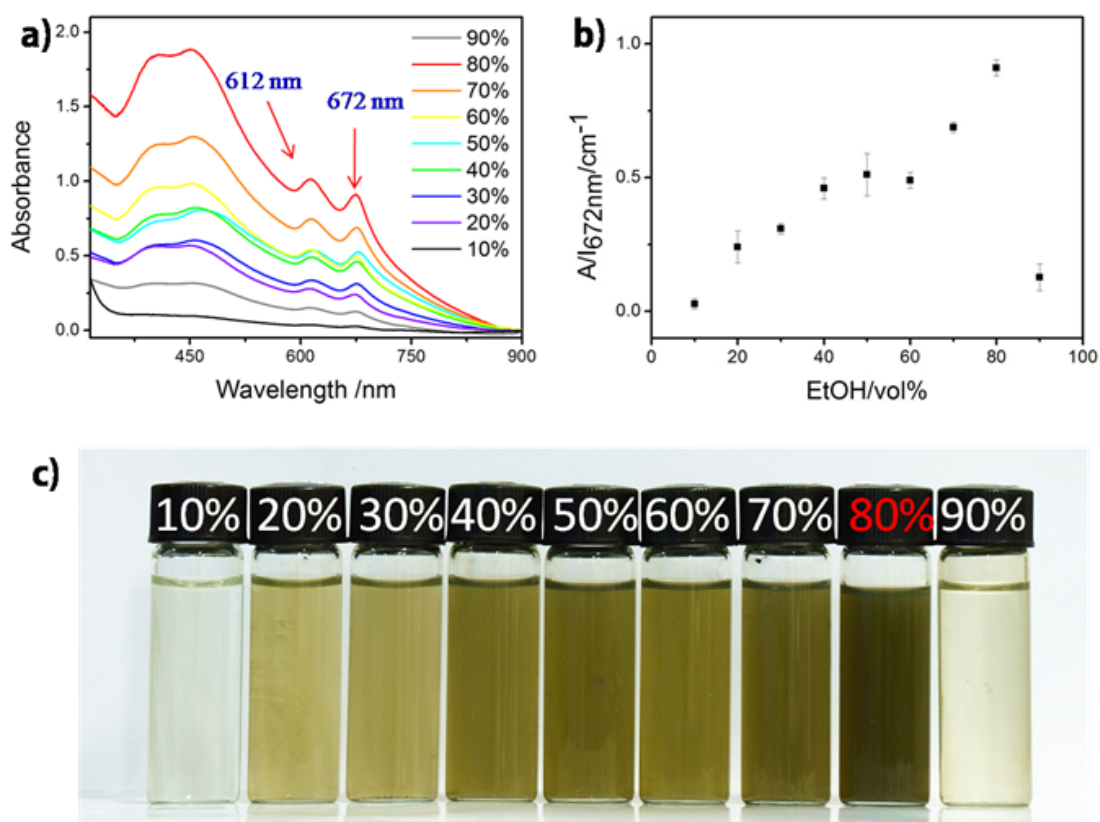


**Figure S3.** Optical characterization of MoS<sub>2</sub> dispersions. a) Absorption spectra of MoS<sub>2</sub> suspensions with ethanol volume fractions of 10 to 90 % in ethanol. b) The absorbance of the MoS<sub>2</sub> suspensions with different volume fractions of ethanol at the set wavelengths of 672 nm are shown as dots. c) Photographs of MoS<sub>2</sub> suspensions with ethanol volume fractions of 10 to 90 %.

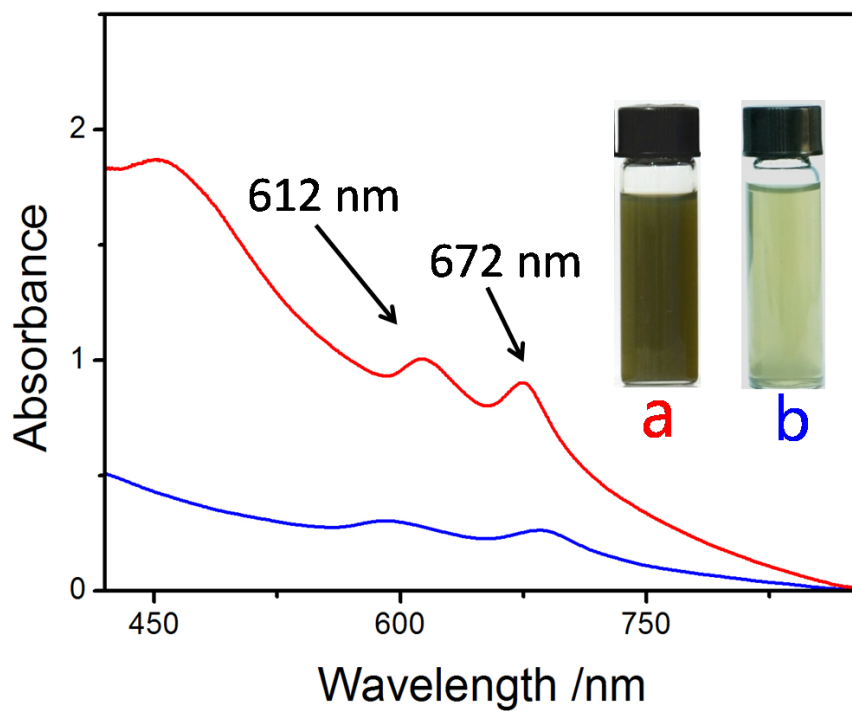


**Figure S4.** Absorption spectra of MoS<sub>2</sub> supernatants, a) MoS<sub>2</sub> supernatants obtained with assistance of SC CO<sub>2</sub> ; b) MoS<sub>2</sub> supernatants obtained without assistance of SC CO<sub>2</sub>.

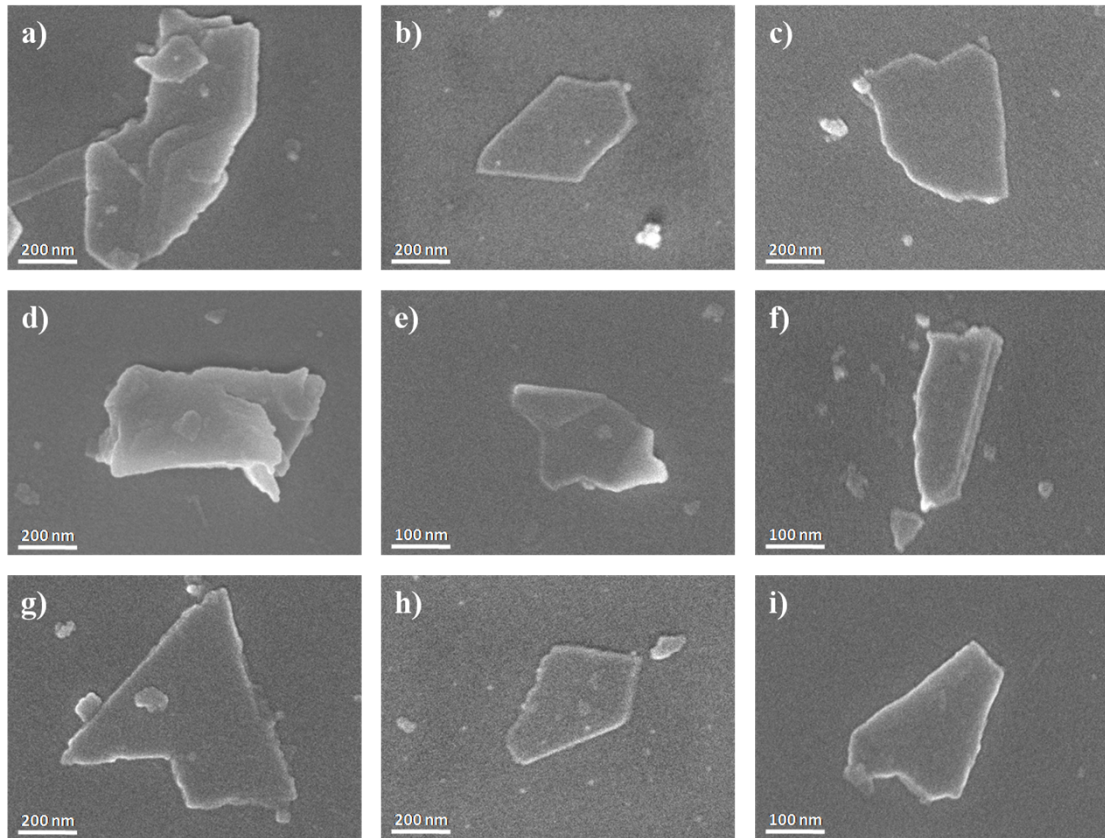


**Figure S5.** SEM images of MoS<sub>2</sub> nanosheets. The images in a-i) show the morphology of MoS<sub>2</sub> nanosheets dispersed in ethanol/water solutions with ethanol volume fractions of 10 to 90 %, respectively.



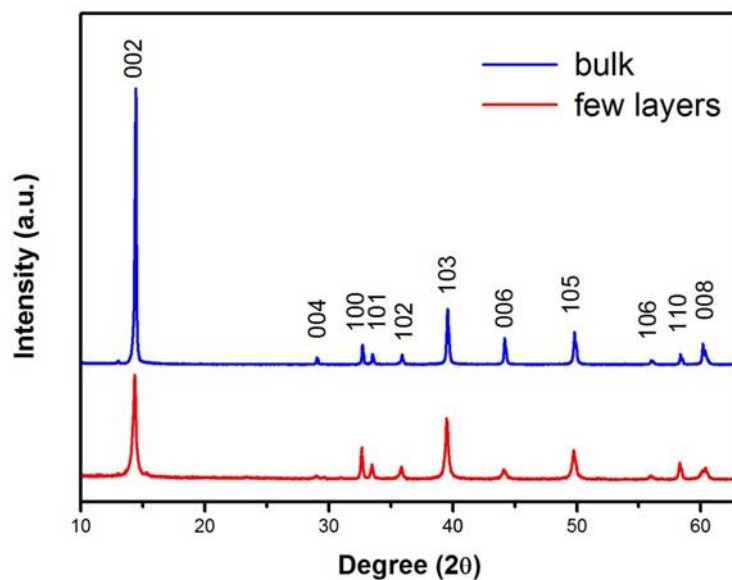


**Figure S6.** XRD patterns of bulk MoS<sub>2</sub> and few layers MoS<sub>2</sub>.

From the X-ray diffraction (XRD) pattern shown in Figure S6, it can be observed that both the MoS<sub>2</sub> nanosheets and bulk powder are identified as 2H MoS<sub>2</sub> with a dominant peak appearing at 14.4, reflecting the (002) plane (ICDD card No.37-1492). Furthermore, the appearance of a strong (002) peak confirms the presence of exfoliated MoS<sub>2</sub> nanosheets with enhanced planar crystal structure.

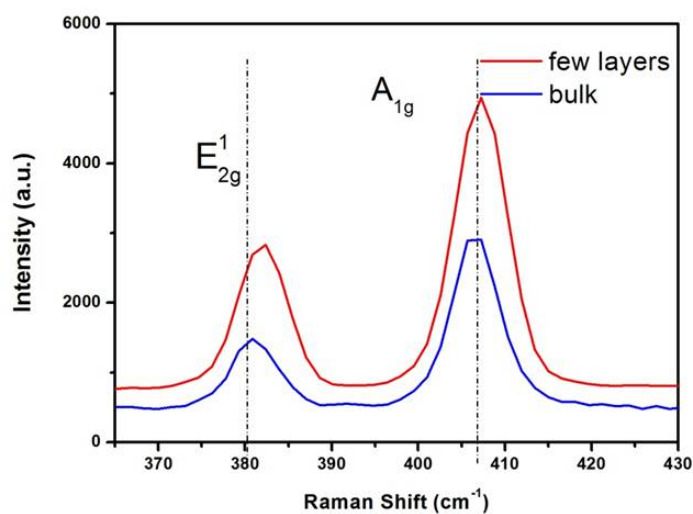


**Figure S7.** Raman spectra recorded using a 536 nm laser for bulk MoS<sub>2</sub> and few layers MoS<sub>2</sub>, where the broadening of the peaks (E<sub>2g</sub><sup>1</sup> and A<sub>1g</sub>) and peak shift indicate the decrease in the number of layers.

Through the Raman mapping of MoS<sub>2</sub> shown in Figure S7, we can confirm that the few-layered MoS<sub>2</sub> sheets were successfully produced. In a comparison of the exfoliated MoS<sub>2</sub> samples with that of the bulk MoS<sub>2</sub>, the bulk MoS<sub>2</sub> samples shows bands at 380.85 (A<sub>1g</sub>) and 407.25 (E<sub>2g</sub><sup>1</sup>) cm<sup>-1</sup>, while the few-layered MoS<sub>2</sub> exhibits the corresponding bands at 382.40 and 407.25 cm<sup>-1</sup>. The shift in the frequency of the A<sub>1g</sub> mode as a function of thickness in the current study is consistent with the transition from surface to bulk layers. The intensities of the bands become significantly enhanced. It can be clearly seen from the Raman map that the full-widths at half-maximum values are obviously increased in the obtained products than in the bulk samples, which are possibly attributed to phonon confinement by facet boundaries.

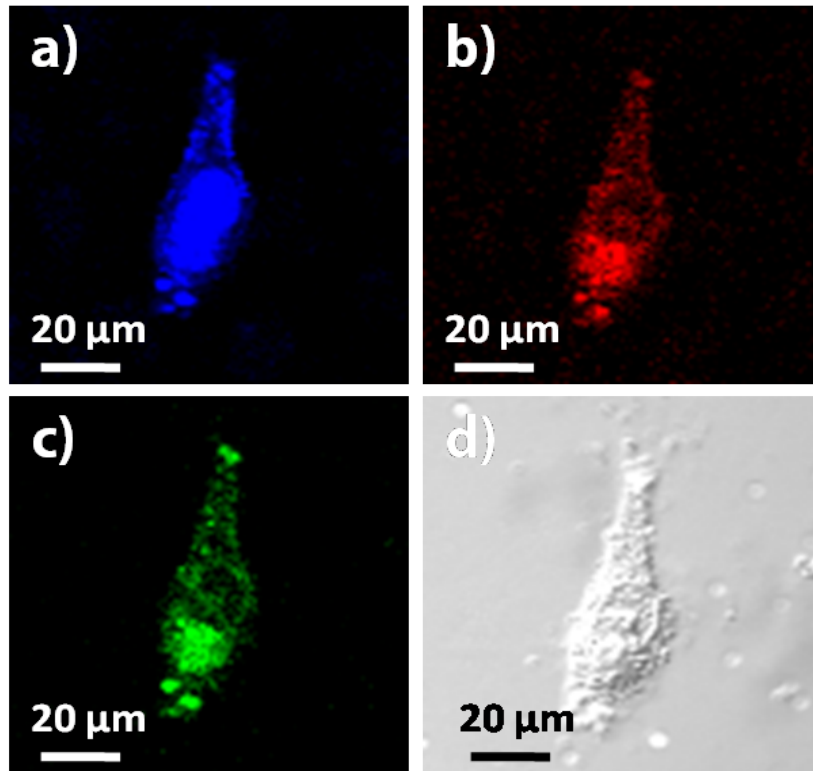


**Figure S8.** The confocal laser scanning microscope images of lung cancer cells stained with MoS<sub>2</sub> nanosheets at broad band excitation light sources of (a) UV (300-400 nm), (b) blue (400-500 nm), and (c) green (500-600 nm).

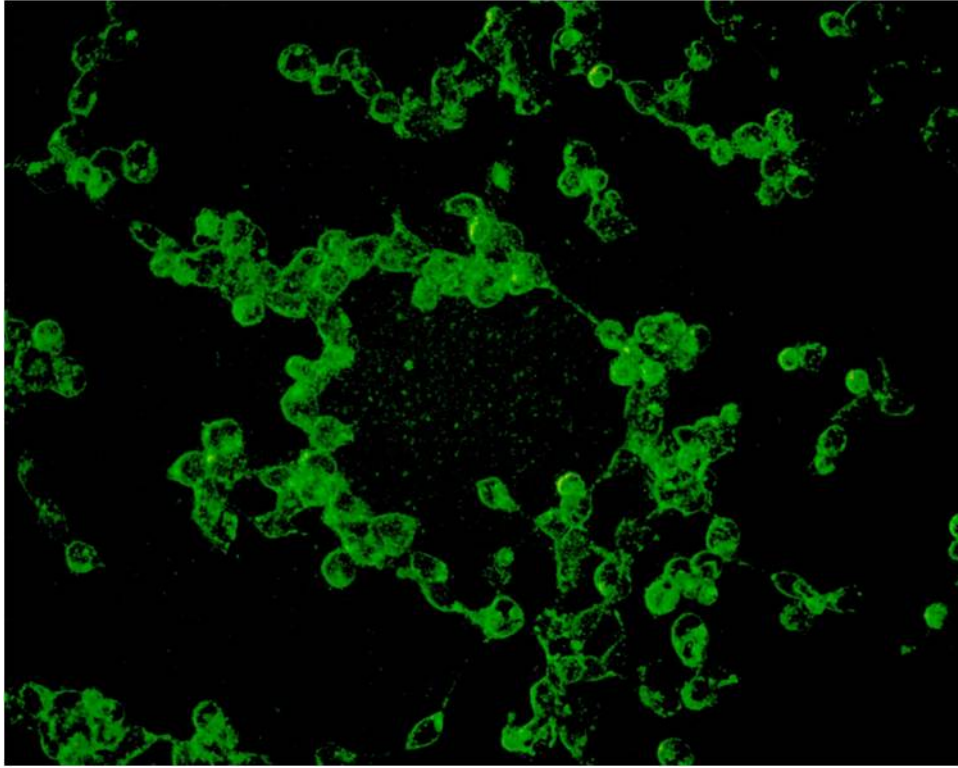


**Figure S9.** The fluorescent images of human embryonic kidney hek 293 cells.